



Shape-optimizing mesh warping method for stereoscopic panorama stitching



Weiqing Yan^{a,*}, Guanghui Yue^b, Jindong Xu^a, Yanwei Yu^a, Kai Wang^a, Chang Tang^c, Xiangrong Tong^a

^a School of Computer and Control Engineering, Yantai University, Yantai 264005, PR China

^b School of Biomedical Engineering, Health Science Center, Shenzhen University, Shenzhen 518060, PR China

^c School of Computer Science, China University of Geosciences, Wuhan 430074, PR China

ARTICLE INFO

Article history:

Received 25 March 2019

Revised 16 September 2019

Accepted 23 September 2019

Available online 24 September 2019

Keywords:

Stereoscopic 3D images

Image alignment

Shape optimization

Stereoscopic panorama

Image stitching

ABSTRACT

In this paper, we propose a novel shape-optimizing mesh warping method for stereoscopic panorama stitching, which aims to resolve shape distortion and unnatural rotation of traditional stitching methods, simultaneously coping with the challenges, misalignment, and stereoscopic inconsistency. Specifically, based on the grid mesh analysis of projective warping, we propose a differential warping method by gradually changing the inclination angle of each mesh line in non-overlapping regions of the image to reduce shape distortion and unnatural rotation. Furthermore, an extended moving direct linear transformation method is proposed to effectively and robustly improve alignment accuracy and maintain stereoscopic consistency in multiple stereoscopic images. Finally, a consistent seam based on the matched feature points in the left- and right- view images of a stereoscopic image is designed to blend images and generate a stereoscopic panorama image. Experiments demonstrate that the proposed method has a superior performance compared to previous methods.

© 2019 Elsevier Inc. All rights reserved.

1. Introduction

Stereoscopic media provides an immersive viewing experience by providing a perception of depth. With an additional depth dimension, more challenges and constraints emerge when creating enjoyable 3D experiences. One such challenge involves creating wide-angle stereoscopic images. Given the limitation of imaging equipment, it is difficult to capture a wide-angle view image in a single camera shot. Image stitching methods [2,21,22] can stitch adjacent images with a small-angle view into a single image with a wide-angle view, and this technology has been extensively examined. However, currently, most stitching methods focus on generating 2D wide-angle images/videos, while the generation of stereoscopic wide-angle images remains a challenging task.

Traditionally, image stitching is implemented via parametric projective warping to ensure image alignment. However, projective warping only provides accurate alignment for planar scenes or parallax-free camera motions [8,20,24]. In other cases, the projective warping method causes misalignment or ghosts [2,19,21,22,28]. Moreover, as a global warping model, projective warping can cause shape distortion in non-overlapping regions of the image. To resolve image alignment issues, several

* Corresponding author.

E-mail address: wqyan@tju.edu.cn (W. Yan).

fine-tuning transformation models [13,16,27,30–32] are introduced. Although they achieve high-precision local alignment, these methods cause shape distortion in non-overlapping regions. To cope with shape distortion, state-of-the-art methods [4,9,14,15,25,26] employ a transition warping method from projective warping to similarity warping in non-overlapping regions. However, unnatural rotation and scaling still occur when stitching multiple images to generate a panorama image.

In this paper, we present a novel shape-optimizing mesh warping method for stereoscopic panorama stitching that can simultaneously cope with these challenges, including shape distortion and unnatural rotation, misalignment, and stereoscopic inconsistency. The contributions of this paper are summarised as follows:

- (1) Based on the grid mesh analysis, we propose a differential warping method to alleviate shape distortion and non-uniform scaling. The proposed differential warping method optimizes the image grid mesh vertices at the non-overlapping regions by gradually changing the inclination angle of horizontal and vertical mesh lines. Compared with other stereoscopic images stitching methods, the proposed method provides less shape/size distortion, and less rotation accumulation; and more image information for stereoscopic panorama images.
- (2) Based on our differential warping method, we extend moving direct linear transformation (MDLT) model to locally refine stereoscopic image alignment and maintain stereoscopic consistency. Compared with current stereoscopic image alignment methods, the proposed method avoids image salient content detection, provides more accurate alignment, and preserves stereoscopic consistency, which benefits multiple stereoscopic image stitching.
- (3) We propose a consistent minimum energy seam by matched feature points in image overlaps. This is an important complement of the proposed warping model that ensures the consistency of whole stereoscopic images in the process of blending.

The remainder of the paper is organised as follows: Section 2 provides a brief overview of related studies. Section 3 introduces a few basic concepts that support the proposed method. In Section 4, we describe the details of the proposed shape optimizing mesh warping method for stereoscopic panorama stitching. The experimental results are presented in Section 5. Finally, the conclusions of this paper are provided in Section 6.

2. Related work

2.1. Image alignment

To resolve misalignment issues, state-of-the-art approaches [9,13,14,16,27,30–32] employ local fine-tune warping to achieve high-precision local alignment. Lin et al. [16] introduced a smoothly varying affine (SVA) field to achieve local adaptive image stitching while maintaining global affinity. Zaragoza et al. [30] proposed an as-projective-as-possible (APAP) image stitching with the moving direct linear transform (MDLT) method, which create multiple local parametric warps for better alignment accuracy. Zhang et al. [31] proposed a hybrid alignment model that combines homography and content-preserving warping to provide flexibility for handling parallax. Li et al. [13] proposed a parallax-tolerant image stitching method based on robust elastic warping, which simultaneously achieved accurate alignment and efficient processing. Li et al. [14] proposed a dual-feature warping for motion model estimation that combined line segments and points to estimate global homography. Joo et al. [9] introduced line correspondences into the local warping model, however, this technique requires user annotations of the straight lines, and the parameter settings are complex. However, the above methods are designed for the alignment of 2D image stitching, and they are therefore not suitable for stereoscopic image stitching. With regard to stereoscopic images, Zhang et al. [32] and Yan et al. [27] proposed stereoscopic image stitching method based on the image's salient content to locally refine alignment and maintain stereoscopic consistency. Since salient content detection is complex, the complexity of stereoscopic image panorama generation would be added if their alignment methods are applied to multiple stereoscopic image stitching. Moreover, these methods are not suitable for stereoscopic panorama images since shape distortion is ignored.

2.2. Shape optimization

To cope with shape distortion, state-of-the-art methods [4,15,25,26] employ a transition warping method from projective warping to similarity warping in a non-overlapping region. Chang et al. [4] proposed shape-preserving half-projective (SPHP) warping for image stitching, which adopts projective warping to align images and similarity transformation to achieve a gradual change from projective to similarity warping across the image. This method significantly reduces distortions and preserves the image shape. However, it can introduce unnatural image rotation and structure deformations, such as line distortions, in cases where the scene is dominated by line structures. Lin et al. [15] proposed an adaptive as-natural-as-possible warping, which linearised the homography in the non-overlapping regions and combined homographies with a global similarity transformation by a direct and simple distance-based weighting strategy to mitigate shape distortion. Xiang et al. [26] proposed line-guided local warping with a global similarity constraint method to reduce shape distortion for image stitching. The line-matching framework exhibits evident advantages, however it suffers from high computational complexity, which restricts its application. Wang et al. [25] proposed a natural shape-preserving stereoscopic image stitching method based on the SPHP warping method. Similarity warping is affected by projective warping, which is subject to unnatural rotation and scaling in the stitching of multiple images.

3. Review of a few basic ideas

In this section, we briefly introduce basic image stitching that supports the description of our method, including image alignment by the projective warping model and the moving direct linear transformation (MDLT) model.

3.1. Projective warping

Projective warping maps a point to another and is used in image stitching. We assume that $(f_k = (f_x, f_y)^T, f'_k = (f'_x, f'_y)^T)$ corresponds to the k th pair of matched points [5,18] in image L1 and L2. They are mapped by projective warping \mathbf{H} with eight parameters, i.e., $f'_k = \mathbf{H}\tilde{f}_k$, where \tilde{f}_k ($\tilde{f}_k = (f_x, f_y, 1)^T$) is f_k in homogeneous coordinates. The expression is expressed as the implicit condition $f'_k \times \mathbf{H}\tilde{f}_k = \mathbf{0}$, it is written as follows:

$$\begin{aligned} & \begin{bmatrix} \mathbf{0}_{1 \times 3} & -f_x & -f_y & -1 & f'_x f_x & f'_y f_y & f'_y \\ f_x & f_x & 1 & \mathbf{0}_{1 \times 3} & -f'_x f_x & -f'_x f_y & -f'_x \\ -f'_y f_x & -f'_y f_y & -f'_y & f'_x f_x & f'_x f_y & f'_x & \mathbf{0}_{1 \times 3} \end{bmatrix} \begin{pmatrix} \mathbf{h}_1 \\ \mathbf{h}_2 \\ \mathbf{h}_3 \end{pmatrix} = \mathbf{0} \\ & \mathbf{H} = \begin{pmatrix} h_{11} & h_{12} & h_{13} \\ h_{21} & h_{22} & h_{23} \\ h_{31} & h_{32} & 1 \end{pmatrix} = \begin{pmatrix} \mathbf{h}_1 \\ \mathbf{h}_2 \\ \mathbf{h}_3 \end{pmatrix} \end{aligned} \quad (1)$$

Since only two of the rows are linearly independent, we choose the first -two rows of the above equation, that is:

$$\begin{aligned} & \begin{bmatrix} f_x & f_y & 1 & \mathbf{0}_{1 \times 3} & -f_x f'_x & -f_y f'_x \\ \mathbf{0}_{1 \times 3} & f_x & f_y & 1 & -f_x f'_y & -f_y f'_y \end{bmatrix} \mathbf{h} = \begin{bmatrix} f'_x \\ f'_y \end{bmatrix}, \\ & \mathbf{h} = (h_{11} \quad h_{12} \quad h_{13} \quad h_{21} \quad h_{22} \quad h_{23} \quad h_{31} \quad h_{32})^T \end{aligned} \quad (2)$$

The direct linear transform (DLT) is a basic method to estimate \mathbf{H} from a set of matched points using the linear component, i.e., using two of the rows from Eq. (1). Specifically, DLT is simplified as follows:

$$A_k \mathbf{h} = f'_k, A_k \in R^{2 \times 8}, \mathbf{h} \in R^{8 \times 1} \quad (3)$$

The above equation is a overdetermined equation, which may be estimated by the least square method. The expression is denoted as follows:

$$\mathbf{h}' = \arg \min_{\mathbf{h}} \sum_{k=1}^N \|A_k \mathbf{h} - f'_k\|^2 \quad (4)$$

3.2. Moving direct linear transformation, MDLT

DLT is used to estimate the global transformation \mathbf{h}' from matched points, while MDLT is used to estimate local transformation \mathbf{h}'_{ij} based on feature points and the weight value. Zaragoza et al. [30] proposed as-projective-as-possible warping, i.e., warps that aim to be globally projective, yet allow local deviations with global projective warping. They employed the MDLT method [30] to obtain local transformation \mathbf{h}'_{ij} , which is calculated by the following weighted problem:

$$\mathbf{h}'_{i,j} = \arg \min_{\mathbf{h}} \sum_{k=1}^N \|w_{k,i,j}(A_k \mathbf{h} - f'_k)\|^2 \quad (5)$$

$$w_{k,i,j} = \max \left(\exp(-\|v_{i,j} - f_k\|^2 / \sigma^2), \gamma \right) \quad (6)$$

σ denotes a scale parameter, and γ is used to prevent an excessively low weight value, $\gamma \in [0, 1]$. The point $v_{i,j}$ near the feature points is assigned a higher weight value such that the projective warp \mathbf{h}'_{ij} better respects the local structure. Moreover, as $v_{i,j}$ is moved continuously in the input image, the warp \mathbf{h}'_{ij} varies smoothly. When $v_{i,j}$ is in a data poor or an extrapolation region, the values $\exp(-\|v_{i,j} - f_k\|^2 / \sigma^2)$ are insignificant. This results in point location distortion and consequently image distortion. To avoid this, a small value γ is used to offset the weight and ensure that the image keep the original \mathbf{h} transform in the extrapolation region.

4. Proposed method

In this section, we introduce the proposed shape-optimizing mesh warping method for stereoscopic panorama stitching in detail. Fig. 1 shows the outline of the proposed method. The input images correspond to multiple stereoscopic images, including left view images (L1, L2, L3, L4,...) and right view images (R1, R2, R3, R4,...). To obtain a stereoscopic panoramic image, we sequentially stitch the individual stereoscopic image. First, the adjacent images (L1,R1) and (L2,R2) are aligned

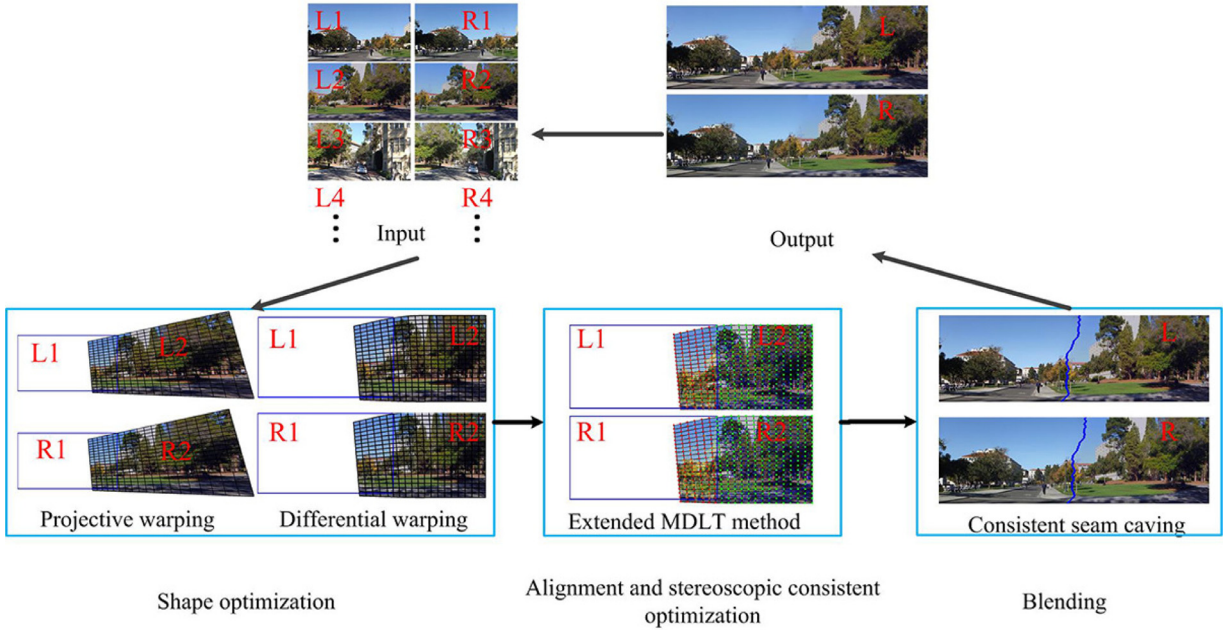


Fig. 1. Outline of the proposed method.

Table 1
Important notations and variables.

Symbol	Definition
$v_{i,j} = (v_x, i, j, v_y, i, j)$	ith row, jth column grid mesh vertex obtained via
$V_{i,j} = (V_{x,i,j}, V_{y,i,j})$	the projective warping method, the differential
$V'_{i,j} = (V'_{x,i,j}, V'_{y,i,j})$	warping method, the Extended MDLT method.
$L_{x,y}(resp. L_{y,x})$	ith row, jth column grid mesh line in horizontal(vertical) direction.
$\theta_{x,y}(resp. \theta_{y,x})$	Inclination angle between line $L_{x,y}(L_{y,x})$ and a horizontal(vertical) line, range from 0° to 90° .
$\Delta\theta_{x,y}(resp. \Delta\theta_{y,x})$	Differential angle at the ith row (jth column)
$\mathbf{V}_0 (resp. \mathbf{V}_0)$	Vertex set at image overlapping (non-overlapping) region.
$(f_{L_2(NO)}, f_{R_2(NO)})$	Matched feature point between left view image L2 non-overlapping region and right view image R2 non-overlapping region.
$F_{L_2R_2} = (f_{L_2}, f_{R_2})$	Matched feature points set between left view image
$F_{L_1L_2} = (f_{L_1}, f_{R_2})$	L2 and right view image R2; L1 and L2; R1 and
$F_{R_1R_2} = (f_{R_1}, f_{R_2})$	R2.
p	First column number of grid mesh in non-overlapping region.
$S_L (resp. S_R)$	A seam in left (right) view image.
$p_L (resp. p_R)$	A point from the seam $S_L(S_R)$.
$p_R(i)$	x-coordinate of point p_R in ith row of seam S_R .
$m (resp. n)$	Total number of rows(columns)in grid mesh cells.

via the projective warping matrix \mathbf{H} , and we use differential warping to optimise projective warping and reduce severe stretching and non-uniform enlargement of non-overlapping regions. Furthermore, based on the shape-optimization image, the extended MDLT method is used to refine the alignment in the overlapping region and maintain stereoscopic consistency. Finally, the target image L1(R1) and the warped image L2(R2) are blended by a minimised consistent energy seam to generate the panorama image L(R). The steps are described in Fig. 1.

4.1. Notations and variables

To facilitate an accurate understanding, a summary of important notations and variables is given in Table 1.

4.2. Shape-optimizing with the differential warping method

In this section, we describe the proposed shape-optimization method. First, given the image alignment between L1(R1) and L2(R2), we initially estimate the projective warping matrix \mathbf{H} via matched feature points. These matched feature points are pruned by an outlier elimination algorithm [6,11]. Here, feature matches are verified by random sample consensus (RANSAC) [6], which is a representative outlier elimination algorithm for image stitching. The proposed method is achieved by a mesh warping technique [17,23,27,32]. The diagram of mesh warping by projective warping is shown in Fig. 2. The

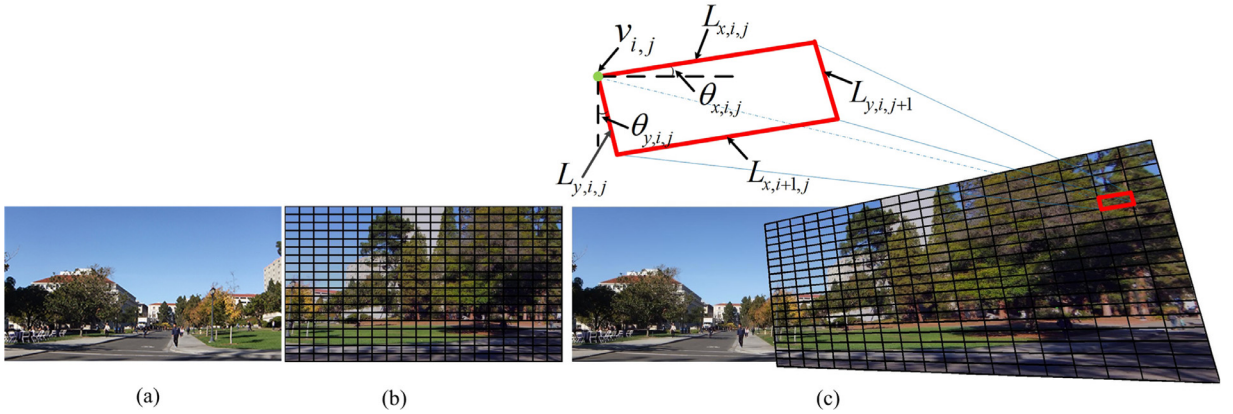


Fig. 2. Grid mesh diagram of image warping; (a) target image L1; (b) image L2 with grid mesh cells; (c) resultant image by warping L2 with projective warping.

input images are divided into $m \times n$ grid mesh cells (Fig. 2(b)). Each grid cell consists of four vertices and four mesh lines, including two horizontal mesh lines and two vertical mesh lines. The grid mesh cells warped by \mathbf{H} and a few important symbols ($v_{i,j}$, $L_{x,i,j}$, $L_{x,i+1,j}$, $L_{y,i,j}$, $L_{y,i+1,j}$, $\theta_{x,i,j}$, $\theta_{y,i,j}$) are shown in Fig. 2(c). As shown in Fig. 2(c), the grid mesh cells in the non-overlapping region are severely distorted in terms of their size and shape.

4.2.1. Differential warping model

To reduce the aforementioned distortion of size and shape, we propose a differential warping method, which gradually changes the inclination angle of horizontal and vertical mesh lines at the non-overlapping regions to update grid mesh vertices. Specifically, we define the differential angle at the horizontal and vertical direction as $\Delta\theta_{x,i}$ and $\Delta\theta_{y,j}$. The inclination angle $\theta_{x,i,j}$ ($\theta_{y,i,j}$) is updated by the following equation:

$$\begin{aligned} \theta_{x,i,j} &= \begin{cases} \theta_{x,i,j-1} - \alpha_i \Delta\theta_{x,i}, & \text{when } \theta_{x,i,j-1} > \delta_1 \\ 0, & \text{otherwise} \end{cases} \\ \theta_{y,i,j} &= \begin{cases} \theta_{y,i-1,j} - \beta_j \Delta\theta_{y,j}, & \text{when } \theta_{y,i-1,j} > \delta_1 \\ 0, & \text{otherwise} \end{cases} \end{aligned} \quad (7)$$

where α_i and β_j denote the scale factors of the differential angle, here, $\alpha_i = \frac{i}{m/2}$ and $\beta_j = \frac{j}{n/2}$. Intuitively, $\theta_{x,i,j}$ gradually decreases when the inclination of the grid mesh line $\theta_{x,i,j-1}$ is larger than δ_1 ; otherwise, the value of $\theta_{x,i,j}$ is zero, i.e., the grid mesh lines eventually trend to the horizontal or vertical line.

To reduce size distortion and maintain the smooth transition from the overlapping to the non-overlapping region, the initial vertices are designed as follows:

$$\begin{cases} V_{x,1,j} = V_{x,1,j-1} + \Delta V_{x,1} \\ V_{y,1,j} = V_{y,1,j-1} + \Delta V_{y,1} \tan(\theta_{x,1,j}) \\ \Delta V_{x,1} = V_{x,1,j-1} - V_{x,1,j-2} \\ V_{i,j} = v_{i,j} \end{cases} \quad j = p, \dots, n. \quad (8)$$

$$i = 1, \dots, m; j = 1, \dots, p-1$$

where $v_{i,j}$ denotes the grid mesh vertex obtained by the projective warping method. p is the first column number of the grid mesh in the non-overlapping region. To reduce size distortion, we designed the same horizontal distance $\Delta V_{x,1}$ between two vertices in the non-overlapping region. Thus $V_{x,1,j} = V_{x,1,j-1} + \Delta V_{x,1}$ $j = p, \dots, n$. When $j = p$, $\Delta V_{x,1} = V_{x,1,p-1} - V_{x,1,p-2}$. Since $v_{1,p-1}, v_{1,p-2}$ are in overlapping region, the horizontal distance between the two vertices in non-overlapping region is the same as that between $v_{1,p-1}$ and $v_{1,p-2}$ in the overlapping region. Based on the initial vertices, the grid mesh size in the non-overlapping region has a smoothly transition from the overlapping region to the non-overlapping region and thus reduces size distortion.

Based on the initial grid mesh vertices and the differential angle, the line expression $L_{x,i,j}$ and $L_{y,i,j}$ are updated, and the new vertex $V_{i,j}$ can be obtained by the line $L_{y,i-1,j}, L_{x,i,j-1}$. The pseudo code of the proposed method is listed in Table 2.

Given the aforementioned procedure, new grid mesh vertices are obtained, and the shape-optimised image is created by the interpolation algorithm [7]. Fig. 3 shows the result of our shape optimization warping. In this Fig. 3(a), green grid mesh cells are obtained by projective warping, and red grid mesh cells are obtained by the proposed differential warping method. In Fig. 3(a), the grid mesh cells obtained by the proposed differential warping method remains consistent with the grid mesh cells obtained by projective warping in the overlapping region, to maintain image alignment. However, in the non-overlapping region, our method alters the inclination angle of the grid mesh line and regularises the sizes of grid mesh

Table 2
Pseudo code of proposed differential warping.

Algorithm 1. Proposed differential warping

1. **Input:** $V_{1,j}$ ($j = p, \dots, n$), $V_{i,j}$ ($i = 1, \dots, m$; $j = 1, \dots, p - 1$) by Eq. (8)
2. **Output:** $\hat{V}_{i,j}$ ($i = 2, \dots, m$; $j = p, \dots, n$)
3. Initialise $i = 2$; $j = p$.
4. **repeat**
5. Update $\theta_{x,i,j-1}$ by Eq. (7). Update $L_{x,i,j-1}$ by $\theta_{x,i,j-1}$ and $V_{i,j-1}$.
6. Update $\theta_{y,i-1,j}$ by Eq. (7). Update $L_{y,i-1,j}$ by $\theta_{y,i-1,j}$ and $V_{i-1,j}$.
7. Update V_{ij} by $L_{x,i,j-1}$ and $L_{y,i-1,j}$ (the intersection of two lines).
8. $i = i + 1$; $j = j + 1$.
9. **until** $i = m$; $j = n$.

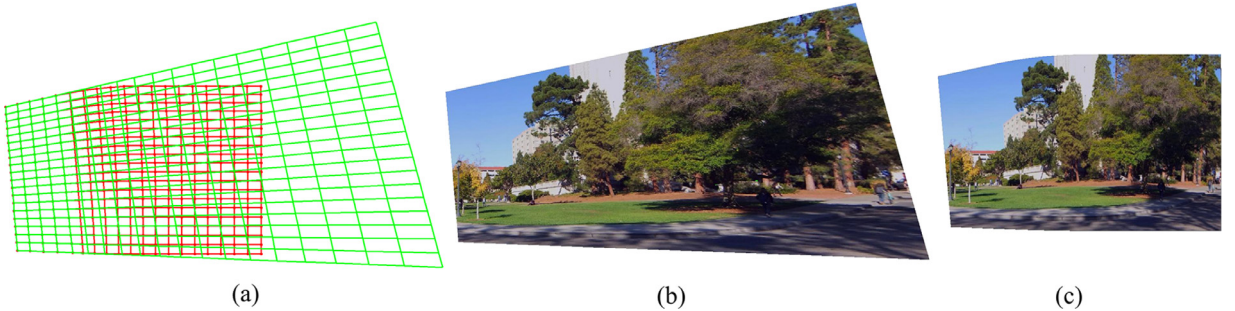


Fig. 3. Shape-optimization mesh warping result. (a) Green grid mesh cells obtained by projective warping, red grid mesh cells obtained by differential warping; (b) warped image L2 by projective warping; (c) warped image L2 by our method. (For interpretation of the references to colour in this figure legend, the reader is referred to the web version of this article.)

cells. From the corresponding warped images (Fig. 3(b) and (c)), we can see that our result (Fig. 3(c)) exhibits lower shape and size distortion than the result of projective warping (Fig. 3(b)) in the image non-overlapping region.

4.3. Alignment and stereoscopic consistent optimization using extended MDLT

The proposed shape-optimizing method can reduce shape distortion and unnatural rotation. However, the shape-optimised images are approximately aligned and stereoscopic inconsistency exists. Hence, a local warping model is required to refine alignment and preserve stereoscopic consistency. Stereoscopic consistency indicates the disparity consistency of stereoscopic images. Hence, the horizontal disparity of corresponding points in left- and right- view images should be consistent with that of shape optimised images; whereas vertical disparities of the corresponding points are zero. Specifically, MDLT as a local warp model can effectuate accurate alignment for 2D images. We extend MDLT to stereoscopic images to obtain more accurate alignment at stereoscopic image overlaps and simultaneously maintain stereoscopic consistency.

As mentioned in Section 3, Zaragoza et al. employed MDLT to fine-tune mesh grid vertices at image overlapping regions to align the image based on matched feature points, while other mesh grid vertices at non-overlapping regions are preserved as projective to the maximum possible extent. Hence, MDLT obtains accurate alignment at the image overlapping region although it does not preserve stereoscopic consistency for stereoscopic images. To simultaneously align images and preserve stereoscopic consistency, the grid mesh vertices set in warped image L2(R2) are divided into two sets, namely \mathbf{V}_o and $\bar{\mathbf{V}}_o$. The vertex set \mathbf{V}_o includes all vertices in the image overlapping region. $\bar{\mathbf{V}}_o$ includes all vertices in image non-overlapping regions. We use extended the MDLT method to \mathbf{V}_o , to refine alignment; used the DLT method with boundary constraints to $\bar{\mathbf{V}}_o$ to preserve stereoscopic consistency.

In the image overlapping region, the matched feature points in image L1(R1) and L2(R2) are mapped by projective warping $\mathbf{H}_{L2}o$ and $\mathbf{H}_{R2}o$.

$$f_{L_1} = \mathbf{H}_{L2}o f_{L_2}, f_{R_1} = \mathbf{H}_{R2}o f_{R_2} \quad (9)$$

Eq. (9) is converted to Eq. (5). We can obtain $\mathbf{H}_{L2}o$ and $\mathbf{H}_{R2}o$ of each vertex V_{ij} by Eqs. (5) and (6). However, there are discontinuous grid meshes in the boundary between the overlapping and non-overlapping region, since a different homography matrix is applied to these two regions. Based on the reference [31], it is not necessary to perfectly align images across the entire overlapping area; rather, it is only necessary to align images at a local region where we can determine a seam to stitch two images together. Hence, we modify Eq. (6). The weight value at the centre area exceeds the weight value at the boundary vertex, i.e., a more accurate alignment is obtained at the centre area of overlaps when compared to other areas; moreover, the boundary vertices are not subject to a significant change to maintain continuous warping. The weight value

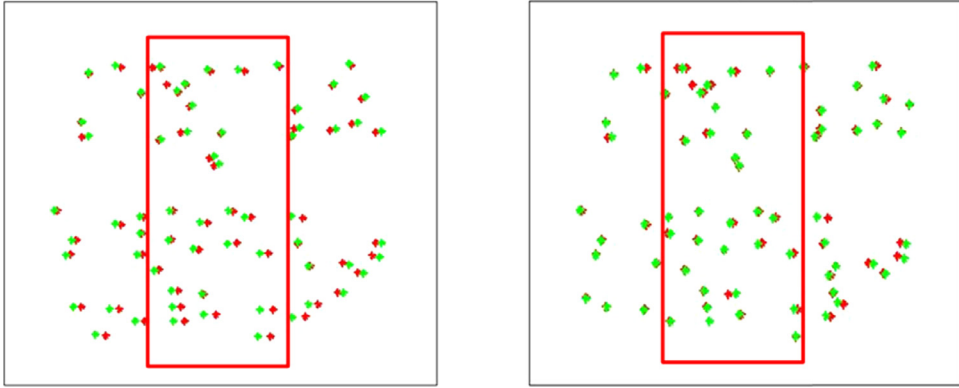


Fig. 4. Alignment results of feature points. (a) Feature points at overlapping region after shape-optimizing warping; (b) feature points at overlapping region after E-MLDT method warping. Note: green points correspond to image L1 and red points correspond to warped image L2. (For interpretation of the references to colour in this figure legend, the reader is referred to the web version of this article.)

$w'_{k,i,j}$ is denoted as follows:

$$w'_{k,i,j} = \exp \left(-\|V_{i,j} - f_k\|^2 \cdot \left\| V_{i,j} - \frac{\sum_{i=1}^m \sum_{j=1}^{p-1} V_{i,j}}{N} \right\|^2 / \sigma^2, \gamma \right), V_{i,j} \in \mathbf{V}_0 \quad (10)$$

Intuitively, the above equation assigns higher weights to data closer to $V_{i,j}$ at the centre of overlaps, and thus the projective warping \mathbf{h}'_{ij} respects the local structure around $V_{i,j}$. In the next section, we use seam selection in the centre area to maintain the image alignment at the image overlapping region.

We combine Eqs. (5) and (10) to obtain the \mathbf{h}'_{ij} of each vertex $V_{i,j} \in \mathbf{V}_0$. \mathbf{h}'_{ij} is solved by updating the weight singular value decomposition(SVD) [30]. The new vertex in the image overlapping region is obtained as follows:

$$V'_{i,j} = \mathbf{h}'_{i,j} V_{i,j} \quad (11)$$

Fig. 4 shows the alignment results of feature points. Green points denote feature points in the image L1, and red points denote feature points in the warped image L2. As shown in Fig. 4(a), severe misalignment is observed after shape-optimizing warping. Conversely, more accurate alignment is observed in the centre region (Fig. 4(b), depicted by red box) where we determine a seam to stitch the image (see next section).

In the non-overlapping region of the image, the vertices are updated by the following DLT method with boundary constraints to maintain stereoscopic consistency. In the stereoscopic image, it is necessary to ensure the vertical alignment of feature points, and thus the y-coordinates of the corresponding feature points in L2 and R2 should be equal. Hence, the y-coordinate of $f_{L_2(NO)}$ and $f_{R_2(NO)}$ are equal, and the value corresponds to $(f_{y,L_2(NO)} + f_{y,R_2(NO)})/2$. We use $f'_{L_2(NO)}$ (resp. $f'_{R_2(NO)}$) to denote the corresponding point of $f_{L_2(NO)}$ (resp. $f_{R_2(NO)}$). The mapping between them is given by the following equation:

$$\begin{aligned} f'_{L_2(NO)} &= \begin{bmatrix} f_{x,L_2(NO)} \\ \frac{f_{y,L_2(NO)} + f_{y,R_2(NO)}}{2} \\ 1 \end{bmatrix}, f'_{R_2(NO)} = \begin{bmatrix} f_{x,R_2(NO)} \\ \frac{f_{y,L_2(NO)} + f_{y,R_2(NO)}}{2} \\ 1 \end{bmatrix} \\ f'_{L_2(NO)} &= \mathbf{H}_{L_2NO} f_{L_2(NO)}, f'_{R_2(NO)} = \mathbf{H}_{R_2NO} f_{R_2(NO)} \end{aligned} \quad (12)$$

To obtain continuous grid mesh vertices, the \mathbf{H}_{L_2NO} and \mathbf{H}_{R_2NO} need to maintain consistency with \mathbf{H}_{L_2O} and \mathbf{H}_{R_2O} in overlapping region, i.e., the vertices $V_{i,p-1}$ in the overlapping region by \mathbf{H}_{L_2O} are consistent with $V'_{i,p-1}$:

$$\begin{aligned} V'_{i,p-1} &= \mathbf{H}_{L_2NO} V_{i,p-1} & V_{i,p-1} \in L2 \\ V'_{i,p-1} &= \mathbf{H}_{R_2NO} V_{i,p-1} & V_{i,p-1} \in R2 \end{aligned} \quad (13)$$

where $V'_{i,p-1}$ denotes the vertex obtained by Eq. (11). Combining Eqs. (12) and (13), we can obtain \mathbf{H}_{L_2NO} and \mathbf{H}_{R_2NO} by singular value decomposition method.

After obtaining the optimised grid mesh vertices from sets \mathbf{V}_0 and $\overline{\mathbf{V}_0}$, we apply the bilinear interpolation algorithm [7] to provide the warped left and right view images.



Fig. 5. Consistent seam. Top: seam in the stitched left view image; Bottom: seam in the stitched right view image.

4.4. Blending based on consistent seam caving

To blend target and warped images, a seam with a minimum difference is selected via the seam-caving method [1] at warped images L1 and the L2 overlapping region. The seam S_L in the left view image is computed as follows:

$$\begin{aligned} e_L &= \|I_{L1} - I_{L2}\| + w_G \|G_{L1} - G_{L2}\| \\ E_{i,j} &= e_L(i, j) + \min(E_{i-1,j-1}, E_{i-1,j}, E_{i-1,j+1}) \end{aligned} \quad (14)$$

where I_{L1} and I_{L2} denote the grey image value at the overlapping regions of the warped images; G_{L1} and G_{L2} denote the gradients of overlapping regions of the warped images. The feature points exhibit more alignment at overlaps, and their matched points are quickly obtained at the right view image. Thus the seam at image R1 and R2 is calculated by matched feature points from the seam S_L . Specifically, we initially determine feature points p_L in S_L from the matched feature points set F_{L_2,R_2} to ensure the feature points p_R are present in the right view image. Furthermore, other points, which are not from the feature point set F_{L_2,R_2} in seam S_R , are confirmed by p_R and their relationship with the points in S_R . The expression of the seam S_R is given as follows:

$$S_R(i) = \begin{cases} p_R(i), p_L(i) \in S_L \quad \text{and} \quad p_L(i) \in F_{L_2,R_2} \\ S_R(i-1) + p_L(i) - p_L(i-1), p_L(i) \in S_L \quad \text{and} \quad p_L(i) \notin F_{L_2,R_2} \end{cases} \quad (15)$$

where $p_L(i)$ denotes the x -coordinate of point p_L in the i th row of seam S_L . We obtain the results for the seam samples via an experiment (Fig. 5). As shown in the figure, a consistent seam exists in the left view image and the right view image.

After the seam is obtained, we use the seam and the multi-band blending algorithm [3] to compose the final left and right view panorama.

5. Experiments

In this section, a few comparative experiments are conducted to demonstrate the advantages of the proposed method. Since there is only one stereoscopic image set captured by the stereo camera FUJIFILM 3D for the stereoscopic panorama image in Ref. [32], we casually capture further stereoscopic image sets using the handheld stereo camera FUJIFILM 3D to generate stereoscopic panorama images and compare the results of other methods. Each stereoscopic image set includes multiple left view images and multiple right view images.

5.1. Experimental result comparisons

We conduct experiments comparing our proposed method with other existing methods, including APAP [30], Zhang's method [32], and Wang's method [25]. The APAP method is a representative global projective warping stitching method,



Fig. 6. Comparison results with global projective warping. Top to bottom: input left view images; APAP method result [30]; result of the proposed method.

which addresses the problem of image alignment in a better way compared with the other global projective warping methods. Zhang's method represents a stereoscopic stitching method. Wang's method is a shape-optimization method for stereoscopic image stitching.

Fig. 6 shows the comparison results of APAP [30] and the proposed method. The APAP method could achieve high-precision local alignment by computing a local homography for every image patch. However, the method assumes projective warping as global warping, which causes shape distortion in non-overlapping region. When more images are stitched to further extend the field of view, the non-overlapping region is severely stretched or non-uniformly enlarged. As shown in the second row of Fig. 6, severe distortions are observed in the size and shape. To view or print the panorama image, it is necessary to crop the image to a rectangle. Thus, only the region depicted by the red box (Fig. 6) remains, while other regions are excluded, leading to information loss. Conversely, our method considers reducing the shape and size distortions while stitching two images. The proposed differential warping method optimizes the image grid mesh at the non-overlapping regions by gradually changing the inclination angle of horizontal and vertical mesh lines to reduce shape and size distortion. Thus, minimal shape distortions are noted in the non-overlapping region. From the third row in Fig. 6, shape distortions are minimal; moreover, more information is preserved compared with the result obtained by APAP.

For stereoscopic image stitching, Zhang's method [32] and Yan's method [27] preserve stereoscopic consistency; however, their methods consider projective warping as global warping, which causes shape distortion. We conduct a comparison with Zhang's method [32], and Fig. 7 shows a comparison result. The resulting image (third row in Fig. 7) of Zhang's method is provided on the publication homepage. As shown in the figure, information loss occurs in comparison with input images as the stitched image may be cropped owing to shape distortion. Conversely, the proposed shape-optimizing method aligns the image, reduces shape distortion, and preserves more information.

Fig. 8 shows a comparison of the proposed method with Wang's method, which employs a transition warping method from projective warping to similarity warping to reduce shape distortion. Since the similarity warping is influenced by projective warping, the method is subject to unnatural rotation and causes more information loss while stitching multiple images. As shown in the second row in Fig. 8, although this method reduces shape distortion, unnatural image rotation exists and leads to information loss while viewing or printing the panorama (only the content in the red box remains). In contrast, our differential warping method gradually reduces the inclination angle of horizontal or vertical mesh grid lines in non-overlapping regions until the inclination angle is zero. The proposed method benefits from multiple images stitching without shape distortion and unnatural rotation accumulation. From this figure, we can see the proposed method could reduce shape and size distortion, avoid unnatural rotation, and preserve more information. More quantitative comparison results are shown in Fig. 13 and Tables 3–5.

Figs. 9–12 show the results of the proposed method for stereoscopic panorama images. The proposed method is observed to reduce shape distortion, align the input images without ghost, and maintain stereoscopic consistency, thereby avoiding an uncomfortable viewing experience (Table 4).

5.2. Quantitative evaluation

In this section, we conduct a quantitative analysis to verify the effectiveness of the proposed method. The proposed method is compared with other methods based on four aspects, including the information and the cropped ratios [31], root

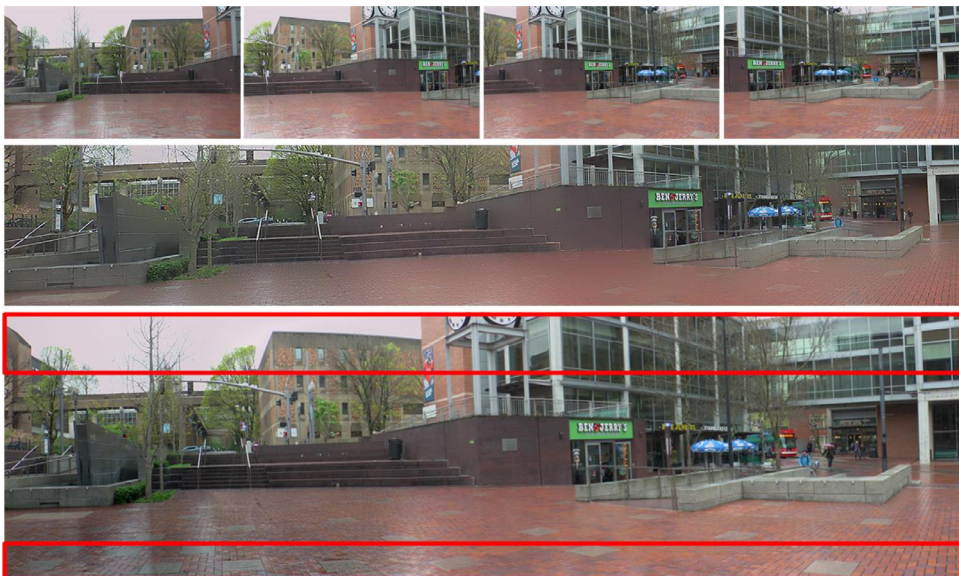


Fig. 7. Comparison of the results with Zhang's method [32]. From top to bottom: input left view images; result of Zhang's method; result of proposed method.

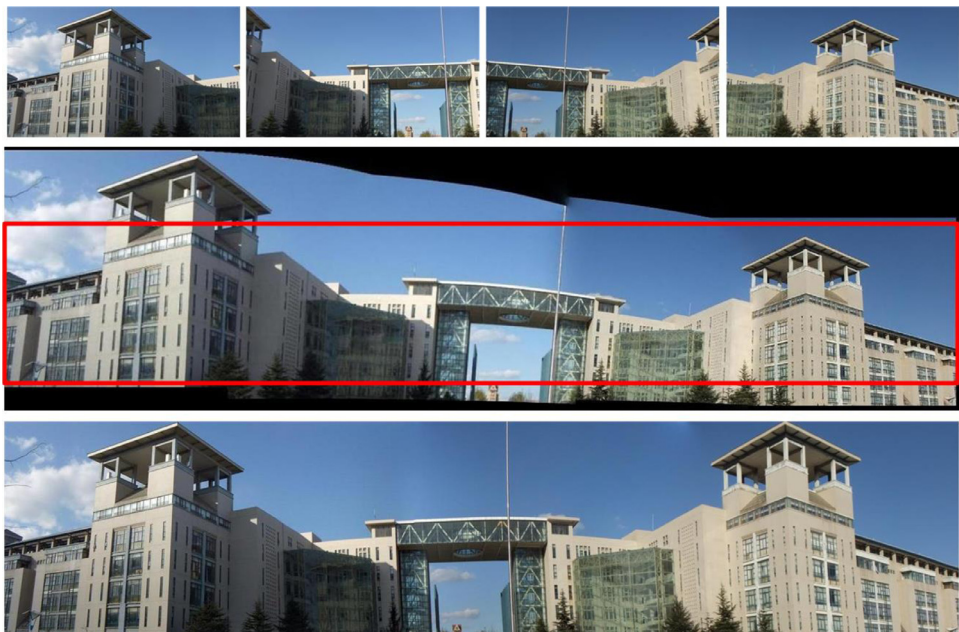


Fig. 8. Comparison of proposed method with Wang's method [25]. Top to bottom: input left view images; result of Wang's method; result of proposed method.

Table 3
RMSE of matched feature points.

Dataset	Fig. 6	Fig. 7	Fig. 9	Fig. 10	Fig. 11(L)	Fig. 11(R)	Fig. 12
APAP	3.26	2.27	1.53	3.04	2.59	2.39	-
Zhang's	4.19	3.45	3.78	4.26	4.43	3.24	-
Wang's	3.22	2.12	2.23	2.98	2.32	2.13	3.60
Proposed	1.55	2.07	1.45	2.02	1.86	2.12	2.77

Table 4

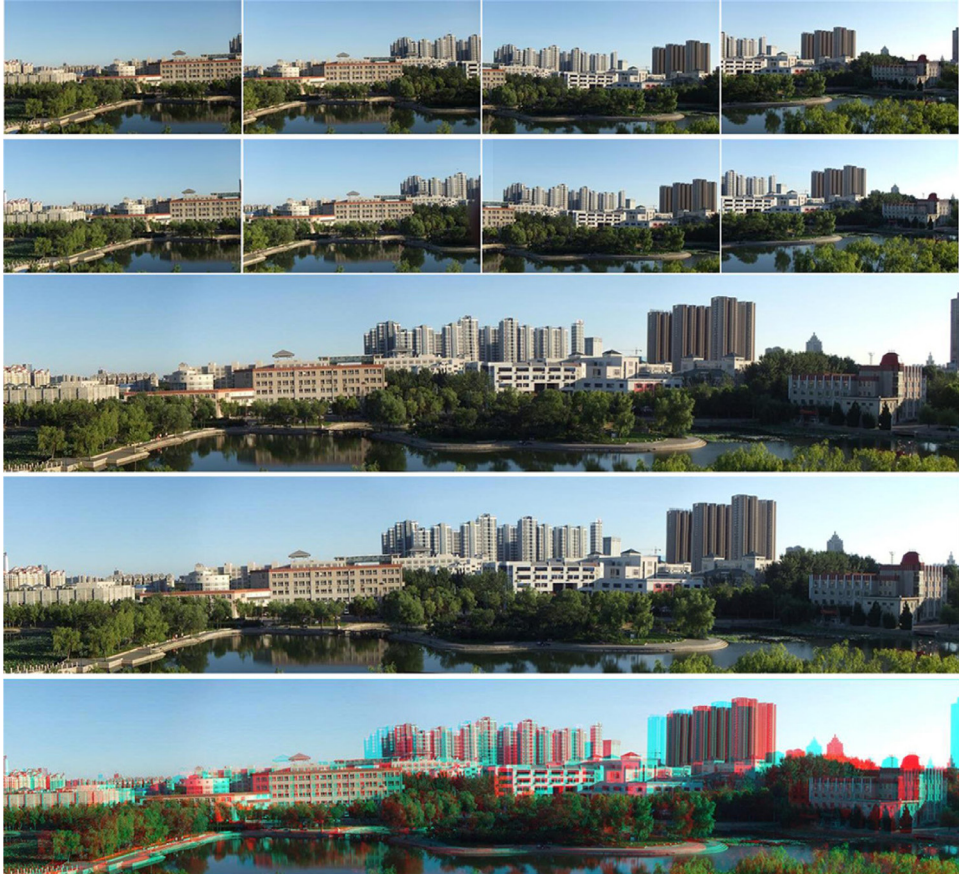
Average absolute vertical disparity(/pixel).

Dataset	Fig. 6	Fig. 7	Fig. 9	Fig. 10	Fig. 11(L)	Fig. 11(R)	Fig. 12
APAP	4.59	5.13	6.15	4.62	3.78	3.56	–
Zhang's	1.34	1.65	1.46	1.23	1.02	1.15	–
Wang's	1.32	1.81	1.41	1.21	1.01	1.20	2.03
Proposed	1.28	1.75	1.39	1.21	0.94	1.07	1.65

Table 5

Average evaluation scores.

Dataset	Fig. 6	Fig. 7	Fig. 9	Fig. 10	Fig. 11(L)	Fig. 11(R)	Fig. 12
APAP	1.09	2.22	2.95	1.96	2.86	2.85	–
Zhang's	1.46	3.29	3.70	2.83	3.69	3.70	–
Wang's	4.03	4.29	4.38	4.09	4.49	4.26	4.14
Proposed	4.73	4.63	4.57	4.22	4.56	4.58	4.52

**Fig. 9.** Stereoscopic panorama stitched results. From top to bottom: input left view images; input right view images; output left view panorama image; output right view panorama image; anaglyph stereoscopic panorama image.

mean squared error (RMSE) of matched feature points [10], average absolute vertical disparity (AVD) [16,20], and a user study [15,16].

According to the comparative method in Ref. [31], we compare the information ratio and the cropped ratio of the stitching result of the proposed method and others. Given images to be stitched, the desired final image should contain as much information as possible. We use the information ratio as an indicator. Since the image is ultimately stored as a rectangular image, an information ratio value that is closer to one will provide more useful information that is used to illustrate the image in the stitched result. Hence, we use cropped ratio to measure useful information. The information ratio I_{fr} and cropped

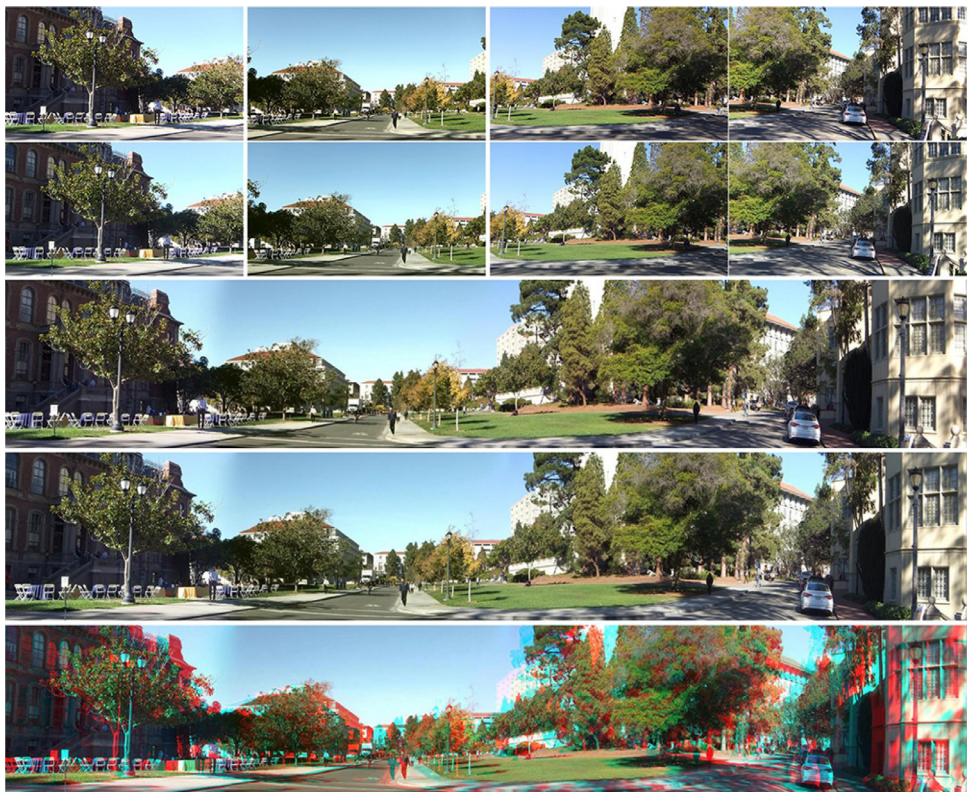


Fig. 10. Stereoscopic panorama stitched results. From top to bottom: identical to Fig. 9.

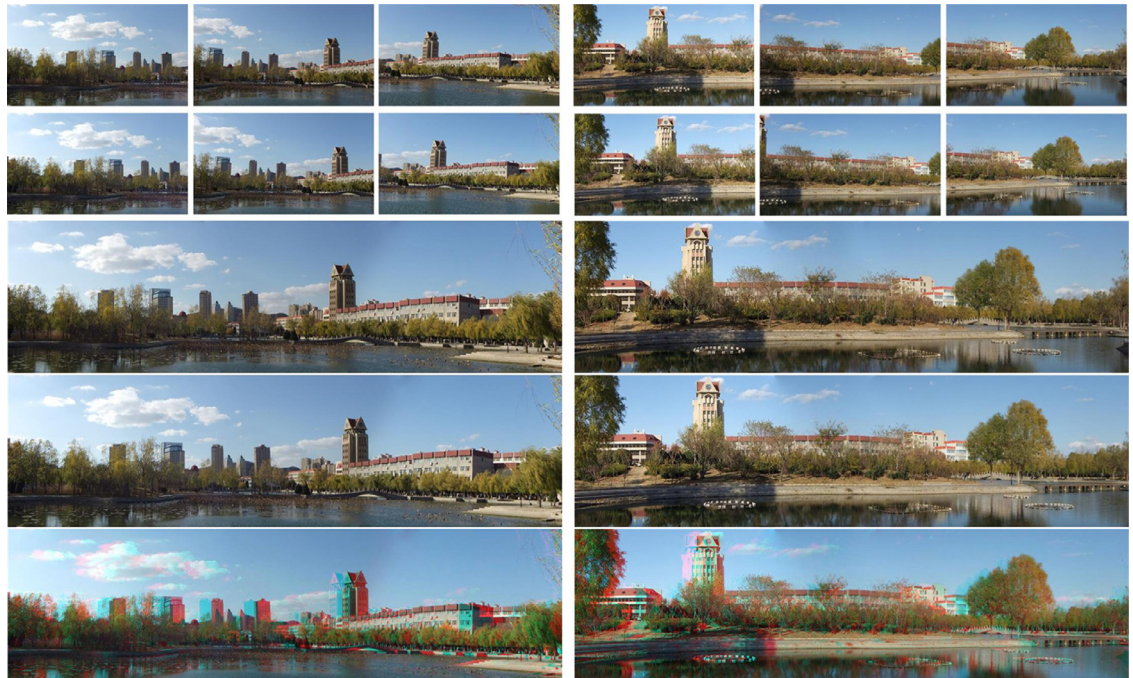


Fig. 11. Stereoscopic panorama stitched results. From top to bottom: identical to Fig. 9.



Fig. 12. Stereoscopic panorama stitched results. From top to bottom: identical to Fig. 9.

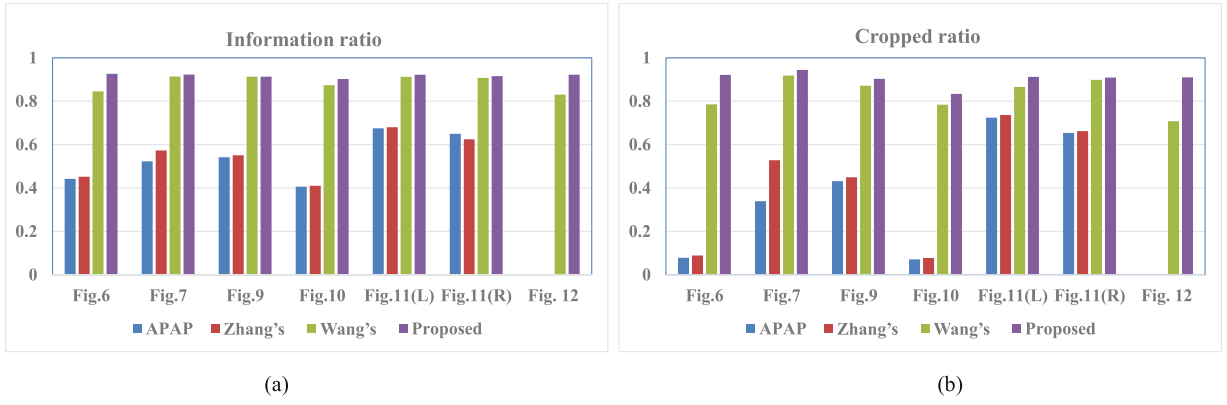


Fig. 13. Comparison of proposed and other methods with respect to information and cropped ratios.

ratio I_{Cr} are defined as follows:

$$I_{lr} = 1 - \frac{N_{blackpixels}}{N_{Stitched}} \quad I_{Cr} = 1 - \frac{N_{Cropped}}{N_{Stitched} - N_{blackpixels}}$$

$$N_{Stitched} = W_{Stitched} \cdot H_{Stitched} \quad N_{Cropped} = W_{Cropped} \cdot H_{Cropped} \quad (16)$$

where $N_{blackpixels}$ is the total number of black pixels (or white pixels) in the background of the stitched result; $W_{Stitched}$ and $H_{Stitched}$ are the width and height of the stitched image, respectively. $W_{Cropped}$ and $H_{Cropped}$ are the width and height of the cropped result, respectively. The information ratio represents the ratio of the remaining pixels except the black pixels in the stitched result to the total number of pixels. The cropped ratio represents the ratio of the information contained in the cropped image to the information of original stitched result. The results of information ratio and cropped ratio are presented in Fig. 13. Since APAP and Zhang's method generate severe shape distortion that prevents image panorama generation when

Table 6
Paired samples *t*-test for user study results.

Pair	Mean(μ)	Std. Deviation(σ)	p-value
APAP & Proposed	2.3217 4.5483	0.7241 0.1727	0.001
Zhang's & Proposed	3.1117 4.5483	0.8793 0.1727	0.013
Wang's & Proposed	4.2567 4.5483	0.1732 0.1727	0.025

more images are stitched for panorama images, there are no corresponding values of Fig. 12 in Fig. 13(a) and (b). As shown in Fig. 13(a) and (b), the information ratio and cropped ratio of APAP and Zhang's method are lower than other methods since their methods assume projective warping as global warping, which causes shape distortion in non-overlapping regions. Wang's method considers shape distortion, and thus the information ratio and cropped ratio are higher than the values of APAP and Zhang's method. However, Wang's method can cause image unnatural rotation, and the values of Wang's method are lower than the values of proposed method. As shown in Fig. 13(a), the information ratio of the proposed method is much higher than that of other methods, which means that our method contains more information in the stitched image. As shown in Fig. 13(b), our method has a higher cropped ratio in comparison to other methods, which means that our method can better retain useful information in the final image.

According to Ref. [10], we use the root mean squared error (RMSE) of matched feature points at centre region of the overlapping region in the left view images L1 and L2 to quantitatively evaluate the quality of alignment in different approaches. Table 3 lists the RMSE of different approaches. Zhang's method employs the traditional global projective warping method to stitch images, which can cause image misalignment. Hence, the values from Zhang's method exceed those of other methods for all images. The APAP method can better address the problem of image alignment compared with the global projective warping method; Wang's method and the proposed method consider image alignment based on the APAP method, hence their values are lower than those of Zhang's method. However, the proposed method assigns higher weights to data closer to the centre of overlaps, and hence has a more accurate alignment at that centre area.

The viewing experience of stereoscopic images is affected by various factors [10,12,29], and there is no general objective measurement of the quality of stereoscopic stitched image. Specifically, vertical disparity affects stereoscopic consistency, and it is widely accepted that large vertical disparity increases visual discomfort. Therefore, the average absolute vertical disparity (AVD) [27] (in pixels) at all feature points is used to evaluate different methods. Table 4 shows the AVD of panorama stitched stereoscopic images. Since APAP and Zhang's method generate severe shape distortion that prevents image panorama creation when more images are stitched together, there are no corresponding values for Fig. 12 in Table 4. As shown in Table 4, the AVD from APAP exceeds that of the proposed method in all the image pairs, because the method does not consider stereoscopic constraints. Zhang's method, Wang's method, and the proposed method all consider stereoscopic consistency, and produce smaller AVD when compared with APAP method. The proposed method considers shape-optimizing warping and avoids unnatural image rotation; thus, it is superior to Zhang's and Wang's method in terms of stereoscopic panorama images.

To verify the effectiveness of the proposed method, we conduct a user study to compare the visual quality of the stereoscopic images obtained by APAP, Zhang's method, Wang's method, and the proposed method. A total of 12 participants with normal stereoscopic vision were invited to participate in the user study. For each sample, input images were placed on the top of the screen (unchanged) and each stitched panorama image obtained by the aforementioned method was placed on the bottom in a random order. The participants were asked if they felt comfortable with the factors, including misalignment, shape distortion, and eye fatigue. Participants rated images from 1 (very uncomfortable) to 5 (very comfortable).

Since APAP and Zhang's method generate severe shape distortion that prevents image panorama creation when more images are stitched together, there are no corresponding values for Fig. 12 in Table 5. As shown in Table 5, the evaluation scores of APAP and Zhang's method are lower than other methods, since APAP produces undesired vertical disparity and shape distortion, which lead to uncomfortable 3D perception. Zhang's and Wang's methods maintain the consistency of input stereoscopic images, which made their scores higher than the scores of APAP. However, Zhang's method can cause shape distortion because of the assumption of projective warping as global warping; Wang's method can cause unnatural image rotation because it takes a transition from projective warping to similarity warping. Hence, their scores are lower than the scores of proposed method.

According to the statistical analysis from Ref. [15], we conduct the significance difference analysis using paired samples *t*-test method. The average scores (μ), the standard deviations (σ), and the *p*-values of the paired two sample *t*-test are listed in Table 6. From this table, we observe that the average evaluation scores of our method are higher than those of other methods, which demonstrates our results deliver a more comfortable 3D viewing experience than the results obtained by other methods. We also observe that all of *p*-values are smaller than 0.05, which demonstrates that the difference between the results obtained by the proposed method and those obtained by other methods is very significant. From these experimental results, we conclude that the proposed method provides more comfortable viewing effects for stitched panorama images by considering shape optimization, image alignment, and stereoscopic consistency.

6. Conclusion

In this paper, we present a novel shape-optimizing mesh warping method for stereoscopic panorama stitching. First, our differential warping method based on the analysis of projective warping mesh grid gradually changes the inclination angle of horizontal and vertical mesh lines in non-overlapping regions to update mesh vertices until the inclination angle is zero. The proposed method solves the problem of shape distortion and unnatural rotation of existing approaches. In addition, we extend the MDLT method to stereoscopic image stitching to simultaneously guarantee image alignment and stereoscopic panorama consistency. Finally, based on matched feature points, we design a consistent seam in left- and right- view images to generate the stereoscopic panorama image. The stitching results are evaluated with experiments involving visual images and quantitative evaluation. Experimental results show that the proposed method successfully reduces shape distortion and avoids unnatural rotation, aligns images, and preserves stereoscopic consistency for stitching multiple stereoscopic images.

Declaration of Competing Interest

We wish to draw the attention of the Editor to the following facts which may be considered as potential conflicts of interest and to significant financial contributions to this work.

We declare that there are no known conflicts of interest associated with this publication and there has been no significant financial support for this work that could have influenced its outcome.

We confirm that the manuscript has been read and approved by all named authors and that there are no other persons who satisfied the criteria for authorship but are not listed. We further confirm that the order of the authors listed in the manuscript has been approved by all of us.

We understand that the Corresponding Author is the sole contact for the Editorial process (including Editorial Manager and direct communication with the office). She is responsible for communicating with the other authors about the progress, submissions of revisions and final approval of proofs. We confirm that we have provided a current, correct email address which is accessible by Corresponding Author and which has been configured to accept email from the office.

Acknowledgement

This work was supported by National Natural Science Foundation of China under Grants 61801414, 61701451, 61572418, Natural Science Foundation of Shandong Province under Grants ZR2017QF006, J18KZ016, ZR2019MF060.

References

- [1] S. Avidan, A. Shamir, Seam carving for content-aware image resizing, *ACM Trans. Graph.* 26 (3) (2007) 1–10.
- [2] M. Brown, D. Lowe, Automatic panoramic image stitching using invariant features, *Int. J. Comput. Vis.* 74 (1) (2007) 59–73.
- [3] P. Burt, E. Adelson, A multiresolution spline with application to image mosaics, *ACM Trans. Graph.* 2 (4) (1983) 217–236.
- [4] C. Chang, Y. Sato, Y. Chuang, Shape-preserving half-projective warps for image stitching, in: Proceedings of the IEEE Conference on Computer Vision and Pattern Recognition, 2014, pp. 3254–3261.
- [5] S. Chen, Y. Shi, Y. Zhang, J. Zhao, C. Zhang, T. Pei, Local multi-feature hashing based fast matching for aerial images, *Inf. Sci.* 442 (2018) 173–185.
- [6] M. Fischler, R. Bolles, Random sample consensus: a paradigm for model fitting with applications to image analysis and automated cartography, *Commun. ACM* 24 (6) (1981) 381–395.
- [7] P. Heckbert, Fundamentals of texture mapping and image warping, in: M.S. thesis, Department Electronic Engineering Computer Science, University California, Berkeley, 1989, pp. 1–50.
- [8] H. Huang, Y. Hung, Panoramic stereo imaging system with automatic disparity warping and seaming, *Graph. Models Image Process.* 60 (3) (1998) 196–208.
- [9] K. Joo, N. Kim, T. Oh, I. Kweon, Line meets as-projective-as-possible image stitching with moving DLT, in: Proceedings of the IEEE International Conference on Image Processing, IEEE, 2015, pp. 1175–1179.
- [10] M. Lambooij, M. Fortuin, I. Heynderickx, W. IJsselsteijn, Visual discomfort and visual fatigue of stereoscopic displays: a review, *J. Imaging Sci. Technol.* 53 (3) (2009) 1–30201.
- [11] I. Lee, M. Mahmood, Adaptive outlier elimination in image registration using genetic programming, *Inf. Sci.* 421 (2017) 204–217.
- [12] F. Li, F. Shao, Q. Jiang, M. Yu, Local and global sparse representation for no-reference quality assessment of stereoscopic images, *Inf. Sci.* 422 (2018) 110–121.
- [13] J. Li, Z. Wang, S. Lai, Y. Zhai, M. Zhang, Parallax-tolerant image stitching based on robust elastic warping, *IEEE Trans. Multimed.* 20 (7) (2017) 1672–1687.
- [14] S. Li, L. Yuan, J. Sun, L. Quan, Dual-feature warping-based motion model estimation, in: Proceedings of the IEEE International Conference on Computer Vision, 2015, pp. 4283–4291.
- [15] C. Lin, S. Pankanti, k. Ramamurthy, A. Aravkin, Adaptive as-natural-as-possible image stitching, in: Proceedings of the IEEE Conference on Computer Vision and Pattern Recognition, 2015, pp. 1155–1163.
- [16] W. Lin, S. Liu, Y. Matsushita, T. Ng, L. Cheong, Smoothly varying affine stitching, in: Proceedings of International Conference on Computer Vision and Pattern Recognition, IEEE, 2011, pp. 345–352.
- [17] F. Liu, Y. Niu, H. Jin, Casual stereoscopic photo authoring, *IEEE Trans. Multimed.* 15 (1) (2012) 129–140.
- [18] D. Lowe, Distinctive image features from scale-invariant keypoints, *Int. J. Comput. Vis.* 60 (2) (2004) 91–110.
- [19] J. Ma, J. Jiang, C. Liu, Y. Li, Feature guided gaussian mixture model with semi-supervised em and local geometric constraint for retinal image registration, *Inf. Sci.* 417 (2017) 128–142.
- [20] C. Richardt, Y. Pritch, H. Zimmer, Megastereo: Constructing high-resolution stereo panoramas, in: Proceedings of the IEEE Conference on Computer Vision and Pattern Recognition, 2013, pp. 1256–1263.
- [21] H. Shum, R. Szeliski, Construction and refinement of panoramic mosaics with global and local alignment, in: Proceeding 6th International Conference Computer Vision, IEEE, 1998, pp. 953–956.
- [22] R. Szeliski, Image alignment and stitching: a tutorial, *Found. Trends Comput. Graph. Vis.* 2 (1) (2007) 1–104.
- [23] C. Tang, J. Wu, C. Zhang, W. Li, Salient object detection via weighted low rank matrix recovery, *IEEE Signal Process. Lett.* 24 (4) (2016) 490–494.

- [24] H. Tang, Z. Zhu, Content-based 3-d mosaics for representing videos of dynamic urban scenes, *IEEE Trans. Circuits Syst. Video Technol.* 22 (2) (2011) 295–308.
- [25] H. Wang, Y. Zhou, X. Wang, L. Fang, A natural shape-preserving stereoscopic image stitching, in: Proceedings of the IEEE International Conference on Acoustics, Speech and Signal Processing (ICASSP), IEEE, 2018, pp. 1812–1816.
- [26] T. Xiang, G. Xia, X. Bai, L. Zhang, Image stitching by line-guided local warping with global similarity constraint, *Pattern Recognit.* 83 (2018) 481–497.
- [27] W. Yan, C. Hou, J. Lei, Y. Fang, Z. Gu, N. Ling, Stereoscopic image stitching based on a hybrid warping model, *IEEE Trans. Circuits Syst. Video Technol.* 27 (9) (2017) 1934–1946.
- [28] F. Yang, M. Ding, X. Zhang, W. Hou, C. Zhong, Non-rigid multi-modal medical image registration by combining with cat swarm optimization, *Inf. Sci.* 316 (2015) 440–456.
- [29] J. Yang, B. Jiang, Y. Wang, W. Lu, Q. Meng, Sparse representation based stereoscopic image quality assessment accounting for perceptual cognitive process, *Inf. Sci.* 430 (2018) 1–16.
- [30] J. Zaragoza, T. Chin, Q. Tran, M. Brown, D. Suter, As-projective-as-possible image stitching with moving DLT, *IEEE Trans. Pattern Anal. Mach. Intell.* 36 (7) (2014) 1285–1298.
- [31] F. Zhang, F. Liu, Parallax-tolerant image stitching, in: Proceedings of the IEEE Conference on Computer Vision and Pattern Recognition, 2014, pp. 3262–3269.
- [32] F. Zhang, F. Liu, Casual stereoscopic panorama stitching, in: Proceedings of the IEEE Conference on Computer Vision and Pattern Recognition, 2015, pp. 2002–2010.